Catalysis Science & Technology

ARTICLE

The curious effects of integrating bimetallic active centres within nanoporous architectures for acid-catalysed transformations

Received 00th January 20xx,
Accepted 00th January 20xx

DOI: 10.1039/x0xx00000x

www.rsc.org/

Matthew E. Potter,[a] Danni Sun[b] and Robert Raja[b*]

The resourceful combination of distinct Mg, Zn and Si active-sites within a single aluminophosphate framework, via simultaneous isomorphous substitution, has afforded unique bimetallic nanoporous heterogeneous catalysts. Unique site-specific interactions have been engineered, at the molecular level, to facilitate catalytic modifications and optimize product yield. By the dextrous incorporation of individual transition-metal active centres, we are able to intricately control the precise nature of the Brønsted acid sites, thereby influencing their catalytic behaviour for the industrially relevant acid-catalysed Beckmann rearrangement of cyclohexanone oxime and isopropylation of benzene.

Introduction

In the modern era of ever-growing demands and restrictions imposed on the chemical industry, the requirement for cleaner and more sustainable production of bulk chemicals is becoming progressively more urgent. Advances in catalysis are attempting to meet these challenges by pursuing a range of possibilities; some by employing more sustainable feedstocks, while others seek to improve existing chemical routes through the use of more effective catalytic materials. Despite the diverse expansion of modern catalysis, it is clear that any significant advances in sustainability will require the development of single-site heterogeneous catalysts that are both versatile and robust for industrial manipulation. This subsequently places significant importance on the design and creation of increasingly intricate active sites at the molecular level, with a view to rationalising structure-activity relationships in our quest for maximising atom-efficiencies and optimising product yields.[1-5]

In the last decade the need to adroitly construct well-defined active centres has prompted a surge in the development of bifunctional and multimetallic heterogeneous catalysts.[6-9] A growing number of examples in the literature describe how the proficient cooperation of different metals may influence the structure-property correlations between the individual active sites and the surrounding support (framework) infrastructure, which may in turn influence the generation of the desired transition-state for facilitating enhanced catalytic turnovers and selectivity.[10-12] Such notions are already well-understood in the field of nanoparticle chemistry[11-13], whereby precise control of active-site location and crystal morphology is the targeted goal. While several synthetic protocols are already well-established to modulate such properties, the deft combination of individual monometallic species at the molecular level is not trivial. However, the rational introduction of a second metal offers a plethora of new synthetic possibilities towards modulating and optimising catalytic performance.[6,10]

While such systems are still under development, current synthetic methods to engineer such versatile catalysts are reliant on precise and meticulous synthetic manipulation[6] or increasingly sensitive and expensive precursors.[12,13] Furthermore, in-order to facilitate a greater industrial compliance and be applicable to a wider-range of catalytic processes, more robust synthetic strategies need to be evolved. In our previous work[14,15] we have shown the benefits of bimetallic substitution, by introducing redox and Brønsted acid active sites within the same framework, to create bifunctional nanoporous aluminophosphate (AlPO) catalysts. By introducing two discrete active sites into the same microporous framework it was shown that, one could perform multi-step or cascade reactions. For example, the direct sustainable production of ε-caprolactam from cyclohexanone using a one-pot method was demonstrated, by combining bimetallic transition-metal ions that were capable of generating oxidative and acidic sites within the same framework architecture.[14-16] This circumvented the need for employing caustic reagents such as oleum, whilst, at the same time, affording minimal waste. This was achieved by simultaneously incorporating redox-active cobalt[17] ions and a silicon Brønsted acid site,[18] in the near vicinity. The initial ammoximation step, involving the conversion of cyclohexanone to its corresponding oxime was catalysed by the redox centres, while the subsequent Beckmann rearrangement of the cyclohexanone oxime to ε-caprolactam occurred at the silicon site.[14-16]

[a] Georgia Institute of Technology, School of Chemical and Biomolecular Engineering, 311 Ferst Drive, Atlanta, GA, 30332-0100, USA.
[b] School of Chemistry, University of Southampton, Highfield, Southampton, Hants, SO17 1BJ, UK; E-mail: R.Raja@soton.ac.uk

Electronic Supplementary Information (ESI) available: [Additional characterisation, catalytic and mechanistic details can be found here]. See DOI: 10.1039/x0xx00000x

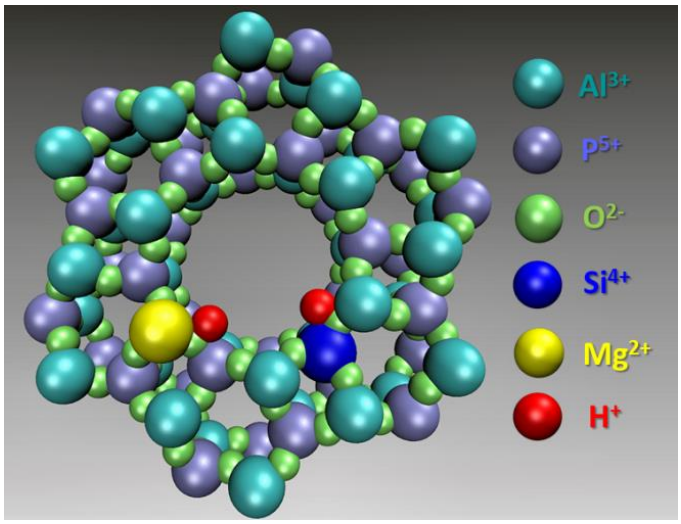

Fig. 1 Graphic illustration detailing bimetallic metal substitution in MgSiAlPO-5.

More recently we have shown that the potential of this synthetic strategy extends beyond bifunctionality. Through rationally extending and modifying solid-state hydrothermal methods, it is possible to engineer novel synergistic interactions between individual metal sites.[19-22] By controlling the relative proximity and location of the two individual species,[19,20] one can prompt metal-metal interactions (when the two are sufficiently close), which can subtly alter the local structural environment of the two species, thereby enhancing their catalytic potential.[20] While such an enhancement requires precise manipulation of active sites at the molecular level, it has been shown that specific metal combinations within AlPO catalysts, has led to synergistic enhancements in for both acid-catalysed (Figure 1) and oxidation reactions.[19-22]

In this present study we explore how induced site-specific interactions can be tailored between different transition-metal active species, for acid-catalysed hydrocarbon transformations, using Mg, Zn and Si-containing AlPO catalysts. The effects of bimetallic substitution are investigated by profiling a multi-reaction catalytic study, which vindicates the potential benefits of creating multimetallic sites for the vapour-phase Beckmann rearrangement of cyclohexanone oxime to ε-caprolactam, and for the isopropylation of benzene to cumene. Notwithstanding the industrial merits of these transformations in the polymer and bulk-chemical industry,[23-25] we also wish to contrast the efficacy of these distinct Brønsted acid sites that arise from the bimetallic substitution. The former reaction (Beckmann rearrangement) shows a preference for weak acid sites, with stronger sites facilitating the formation of coking and ring-opening by-products.[26,27] In stark contrast, the isopropylation reaction requires strong acid sites to activate propan-2-ol, with the weak sites proving inadequate for this process.[28] By contrasting the behaviour of these bimetallic catalysts for these diagnostic reactions, we are able to gain significant insights into the nature and specific acid strength of the active sites within these heterogeneous catalysts.

Experimental

The synthetic protocol for the isomorphous substitution of Mg(II) and Si(IV) into the AFI framework (MgSiAlPO-5) is described (below); an analogous method was employed for the preparation of the monometallic counterparts, details of which are provided in Table 1 (below). The synthesis method to form MgSiAlPO-5 involved initially adding 4.0 g of aluminium hydroxide hydrate (Aldrich) to a homogeneous solution of 5.0 g of phosphoric acid (85% in H_2O, Aldrich) in 20 ml of water and allowing the mixture to stir for 10 minutes. Aqueous homogeneous solutions of 0.33 g of magnesium(II) acetate tetrahydrate (Aldrich) in 10 ml of water and 0.62 g of fumed silica (Aldrich) were added simultaneously to the above solution, which resulted in the formation of a viscous gel, which was stirred for a further 30 minutes in order to obtain a homogeneous mixture. N,N-methyldicyclohexylamine (SDA) (Aldrich) (8.0 g) was then added slowly, followed by 20 ml of water, with vigorous stirring for 60 minutes to obtain a white gel with the composition 1.0Al: 0.85P: 0.80MDCHA: 50H2O: 0.03Mg: 0.20Si.

The contents of the gel were sealed in a Teflon-lined stainless-steel autoclave, which was then transferred to a pre-heated, fan-assisted oven (WF-30 Lenton) that was set to the desired temperature of 190 °C, prior to the onset of the crystallization. The autoclave was heated at 190 °C under autogeneous pressure for 2 hr. The white solid product was collected by filtration, washed with approx. 500 ml deionised water, and dried in air (60 °C) overnight. The as-prepared sample was calcined in a tube furnace under a flow of air at 550 °C for 12 h yielding a white solid. The synthesis procedures of other samples discussed varied only by crystallization temperature and gel composition, which are shown in Table 1.

X-Ray powder diffraction patterns were obtained using a Siemens D5000 diffractometer using Cu $K_{\alpha 1}$ radiation, where λ = 1.54056 Å. Scanning electron microscopy images were obtained using a JEOL-JSM5910 microscope with accelerating voltage of 0.3-30 kV. In this case, the samples were prepared by carbon coating. BET surface area measurements were performed using a Micromeritics Gemini 2375 surface area analyser and prepared using flow-gas preparation. A Perkin-Elmer Optimum 3000 DV was used for ICP analyses, with calcined samples prepared and fully digested in 10 ml of deionised water and 10 ml of ACS Plus Certified H_2SO_4 (Fisher Scientific). Solutions of standard concentrations were used for calibration.

The Beckmann rearrangement of cyclohexanone oxime was performed in a fixed-bed, quartz reactor (4 mm in diameter) with a glass frit, in which a layer of pelletized catalyst (0.25 g) was packed between two layers of glass beads. This was pre-heated by a jacket in the flow-reactor to 673 K under a 20 ml/min flow of helium gas for 1 hour. The temperature was reduced to 573 K and a liquid feed of 300 g/l of cyclohexanone oxime in methanol was fed into the reactor, maintaining a WHSV of 3.3 hr^{-1}, with samples being analysed on an hourly basis (under steady-state conditions). The temperature was then increased to the desired value (598, 623, 648 and 673 K)

Table 1 Synthetic parameters for the synthesis of Mg, Zn and Si-containing AlPO catalysts.

Sample	Molar gel composition	Crystallisation temperature/^{o}C
AlPO-5	1.00P : 1.00Al : 0.75TEA : 25H_2O	200
MgAlPO-5	1.50P : 1.00Al : 0.04Mg : 0.80MDCHA : 60H_2O	200
ZnAlPO-5	1.05P : 1.00Al : 0.04Zn : 0.80MDCHA : 65H_2O	190
SiAlPO-5	0.75P : 1.00Al : 0.25Si : 0.65MDCHA : 40H_2O	200
MgZnAlPO-5	1.50P : 1.00Al : 0.03Mg : 0.03Zn : 0.80MDCHA : 50H_2O	180
MgSiAlPO-5	0.85P : 1.00Al : 0.03Mg : 0.20Si : 0.80MDCHA : 50H_2O	190
ZnSiAlPO-5	0.85P : 1.00Al : 0.03Zn : 0.20Si : 0.80MDCHA : 50H_2O	190

and samples were taken at each temperature after being allowed to equilibrate for an hour. Samples were analysed using a Clarus 400 gas chromatogram with FID and using an Elite 5 column, the peak areas were calibrated using known response factors.

An analogous reactor set up and pre-treatment protocol was employed for the isopropylation of benzene. After pre-treatment at 673 K, the temperature was reduced to 523 K and a liquid feed with 6:1 molar ratio of benzene:isopropanol was employed with a WHSV of 3.5 hr^{-1} under a flow of 10 ml/min of helium gas. Samples were analysed and quantified as described above, conversions were normalised with respect to the molar ratio.

Results and Discussion

Synthesis and Structural Characterisation

The structural integrity of the targeted mono- and bi-metallic samples was confirmed using a range of physico-chemical characterisation techniques. In all samples the intended AFI (AlPO-5) phase was the only AlPO phase present, confirming the integrity of the synthetic procedure, despite the metal incorporation (Figures 2, S1 & S2). The characteristic AFI patterns were examined though Reitveld analysis, which subsequently confirmed that only minimal distortion of the unit cell had occurred. The deviation was quantified as being less than 1% of the undoped-framework parameters in all cases, in concurrence with the small quantities of metal incorporated into the systems (Tables 1, S1 & S2). While subtle, these changes in the unit cell parameters account for the shifts in peak position between the different samples. On closer inspection of the 30-55^{o} range the Zn-containing systems show trace amounts of ZnO within the system, however, given the low intensity of the pattern in this range it is not possibly to quantify the total fraction of the zinc in this state (Figure S2). Furthermore, the relatively smaller channels (7.3 Å) of the AFI architecture would preclude the formation of the ZnO phase within the pores, thereby rendering them invisible to XRD.

The porous nature of the catalytic frameworks was confirmed through volumetric BET analysis, with some systems displaying a prominent deviation from the undoped AlPO-5 system (295.1 to 165.4 $m^2\ g^{-1}$). The reduction in surface area is attributed to the addition of metal dopants modifying the delicate crystallisation kinetics, in some cases forming extra-framework species within the pores, in accordance with powder XRD findings. By applying Scherrer's equation on the 7.4^{o} peak the uniformity of particle sizes was confirmed, as all systems fell within a narrow range of 52-66 nm (Table 2 & S2). This was confirmed through SEM, whereby all systems contained spherical particles of comparable size (10-20 µm) with no visible extra phases present (Figure S3-8). ICP analysis confirmed that the bimetallic samples contain similar metal loadings as the analogous monometallic systems allowing direct comparisons to be made between the catalytic behaviour of the different systems (Table 2 & S1).

Catalytic potential of the monometallic systems

Given the contrasting nature of the acid active site required to perform the isopropylation and the Beckmann rearrangement reactions, the differences in catalytic performance for these reactions is symptomatic of the acid-site strength in the metal-doped AlPO catalysts. Given the concurrence in physical characterisation properties between the different Mg, Zn and Si-containing catalysts, we can attribute any differences in catalytic activity to the direct influence of the individual acid sites.

Table 2: Summary of the textural characterisation properties of Mg, Zn and Si-containing AlPO-5 catalysts.

Sample	Metal loading/wt%			Optimised P6cc unit cell parameters/Å		Specific surface area/$m^2\ g^{-1}$	Particle size/nm
	Mg	Zn	Si	A	c		
AlPO-5	-	-	-	13.69	8.43	295.1	56.5
MgAlPO-5	0.85	-	-	13.71	8.40	193.3	55.5
ZnAlPO-5	-	2.11	-	13.68	8.34	165.4	55.5
SiAlPO-5	-	-	1.69	13.70	8.39	181.9	54.8
MgZnAlPO-5	0.72	1.86	-	13.80	8.41	283.3	66.3
MgSiAlPO-5	0.89	-	1.70	13.68	8.39	168.0	52.6
ZnSiAlPO-5	-	1.33	1.66	13.76	8.40	236.2	64.2

The differing catalytic activity between the MgAlPO-5 and SiAlPO-5 catalysts can be directly correlated to the precise nature of the individual active sites. MgAlPO-5 displays enhanced activity for the isopropylation of cumene (Fig 3B & S10), whilst SiAlPO-5 shows increased specificity for ε-caprolactam in the Beckmann rearrangement (Fig 3A & S9). These observations are consistent with literature findings, confirming that the Brønsted acid sites generated by the inclusion of Mg^{2+} ions into the AlPO framework are strong, and those generated by the isomorphous substitution of Si^{4+} are weaker.[29] The activity profile demonstrated by both of these catalysts in their respective reactions confirms the presence of Brønsted acidity within them. This is a clear indication that the Mg^{2+} and Si^{4+} dopants are isomorphously substituted, as monometallic entities, into the framework of the AFI nanoporous architecture.

In stark contrast the ZnAlPO-5 catalyst appears to be relatively inactive for both reactions, suggesting little to no Brønsted acid sites are present in this material. Given the significant Zn content of the monometallic ZnAlPO-5 catalyst (Table 2) and the relatively inert catalytic performance, it must be concluded that, unlike the Mg^{2+} and Si^{4+} species, the Zn^{2+} ions have not undergone framework substitution, but instead form extra-framework species. It is therefore concluded that the strength of the framework acid site formed is strongly dependant on the nature and type of metal dopant. Further, it is noted that, despite the similar valency and size of the Mg^{2+} and Zn^{2+} ions, the nature of the metal strongly influences the crystallisation kinetics that determines whether the dopant is isomorphously substituted into the framework, or instead, exists as an extra framework site.

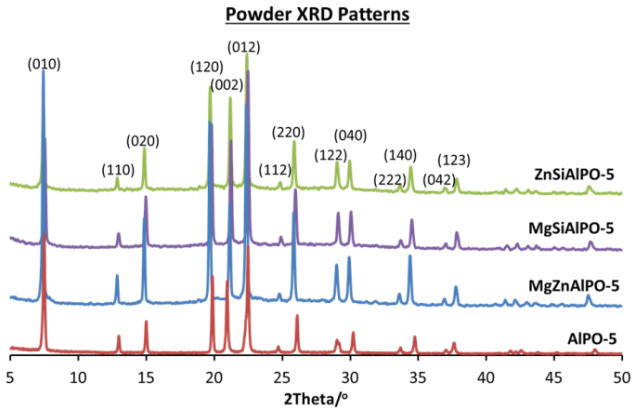

Fig 2. Powder XRD patterns of the novel bimetallic Mg, Zn and Si-containing AlPO-5 catalysts.

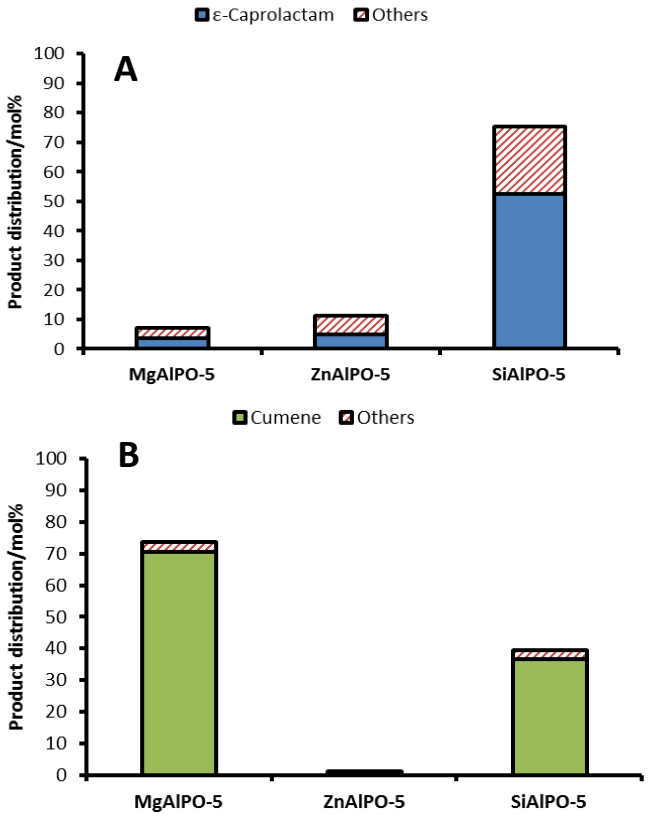

Fig 3 Activity of monometallic catalysts on the vapour-phase Beckmann rearrangement (A) and isopropylation of benzene (B). Conditions: A) WHSV 3.3 hr-1, Helium carrier gas flow 20 ml/min, 0.3 g of catalyst, liquid feed 300g/l of cyclohexanone oxime in methanol, temperature 673 K. B) WHSV of 3.5 hr-1, Helium carrier gas of 10 ml/min, feed 6:1 mole ratio of benzene:isopropanol, temperature 523 K.

Designing bimetallic catalysts – Engineering synergy between Mg^{2+} and Si^{4+}

Direct comparison of the bimetallic Mg(II)Si(IV)AlPO-5 with its analogous monometallic counterparts (Mg(II)AlPO-5 and Si(IV)AlPO-5) reveals distinct differences in catalytic performance. MgSiAlPO-5 catalyst shows a greater specificity for the target product in both reactions, producing a greater ε-caprolactam yield than the SiAlPO-5 system, and a superior cumene yield, compared to the MgAlPO-5 system (Fig 4A, 4B, S11 & S12). Thus adding strong sites to SiAlPO-5 enhances the Beckmann rearrangement, whilst adding weaker sites to MgAlPO-5 aids the formation of cumene. Initially this result appears counter-intuitive, when considering previous work[26-28] on these reactions. The presence of strong-acid sites in the Beckmann rearrangement is known to facilitate coking, ring-opening by-products and the irreversible binding of the oxime inside the pores, all of which would diminish the overall activity and specificity of the system. Further the presence of weak acid sites in the isopropylation of benzene would simply be insufficient to deprotonate the isopropanol to form the active propylene intermediate.

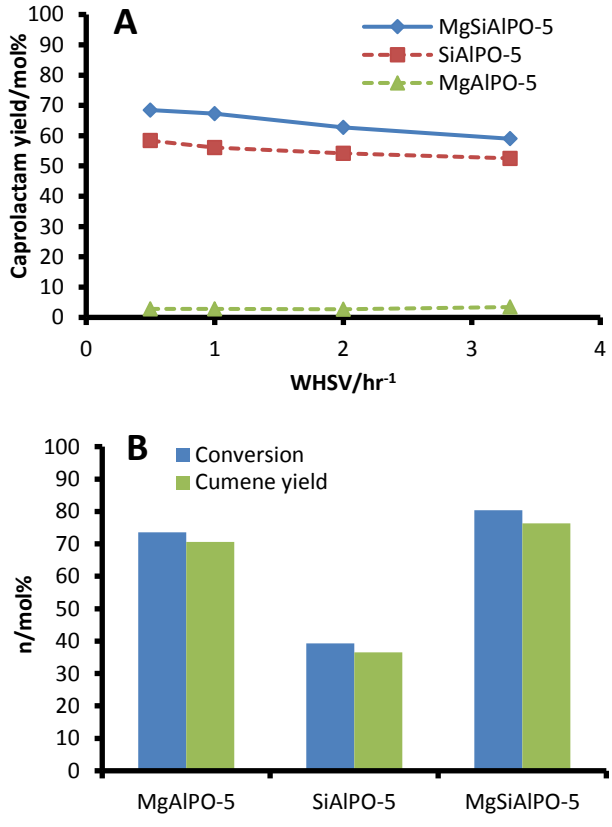

Fig 4. Synergistic enhancement of the Mg(II)Si(IV)AlPO-5 catalyst on the vapour-phase Beckmann rearrangement (A) and isopropylation of benzene (B). Conditions: A) Temperature 673K, Helium carrier gas flow 20 ml/min, 0.3 g of catalyst, liquid feed 300g/l of cyclohexanone oxime in methanol, WHSV as shown. B) WHSV of 3.5 hr^{-1}, He carrier gas of 10 ml/min, feed 6:1 mole ratio of benzene:isopropanol, temperature 523 K.

However, the above are only applicable when considering one type of active site. Careful consideration of the mechanistic pathways of both reactions[26-28] offers a viable explanation for our catalytic trends. Whilst the rate-determining steps comply with established literature examples as stated above, it is worth noting that in both mechanisms there are multiple steps which are acid-catalysed (Figures S17 & S18). It is hypothesised that within each of these mechanisms there is a step which requires a weak acid site and one which requires a stronger acid site. Thus by introducing both types of acid sites into the same material, and thus in relatively close proximity,[30] one improves the efficiency of multiple reaction steps. This then facilitates the subtle catalytic improvements observed experimentally in the bimetallic MgSiAlPO-5 catalyst, explaining the improved product yields and synergistic enhancements seen.

Designing bimetallic catalysts – The peculiar role of zinc

With the Zn(II)AlPO-5 proving to be inactive for both reactions, alloying it with the contrasting Mg(II) and Si(IV) species provoked interesting catalytic responses. It could be expected that, as zinc exclusively occupies extra-framework positions within the AFI architecture, it would serve to retard and hinder the activity of the MgAlPO-5 and SiAlPO-5 catalysts. However through analogous catalytic testing this was found not to be the case. Given the similarity in Mg and Si content in the appropriate monometallic and bimetallic species (Table 2), one can directly attribute the differences in catalytic behaviour between the two catalysts, to the introduction of zinc into the system. Contrasting the performance of the MgZnAlPO-5 and MgAlPO-5 catalysts (Figures 5A, 5B, S13 & S14), one can see a drastic decrease in activity for the isopropylation of cumene, as expected, for the former. Though conversely, in the Beckmann rearrangement, when considering the range of 623-673 K, a substantial increase in catalytic efficacy is noted for the MgZnAlPO-5. As zinc itself proved to be catalytically inactive (Figure 3), it is concluded that this behaviour is due to a modulation of the Brønsted acid site, that is brought about by the isomorphous substitution of magnesium into the AlPO-5 framework. Specifically, the zinc is weakening the magnesium Brønsted acid sites, relative to those present in MgAlPO-5, thereby explaining the catalytic behaviour witnessed. Similarly, contrasting the SiAlPO-5 and ZnSiAlPO-5 catalysts, demonstrates the opposite trend. The addition of zinc to form the bimetallic ZnSiAlPO-5 species shows a significant increase in cumene yield, in the isopropylation reaction (Figures 5C & S16), though a subtle decrease in the yield of ε-caprolactam is noted (Figure 5D & S15). In this case, it would appear that the zinc has strengthened the Brønsted acid sites generated by silicon in the ZnSiAlPO-5 material, relative to the monometallic SiAlPO-5 catalyst. The stronger acid sites are able to more effectively dehydrate the isopropanol reagent, thus resulting in higher yields of cumene. The same (stronger) sites may also anchor the reagents and products in the Beckmann rearrangement, blocking both the active sites and access to the 1D-channels, lowering the yield of ε-caprolactam, as seen in Figure 5D.

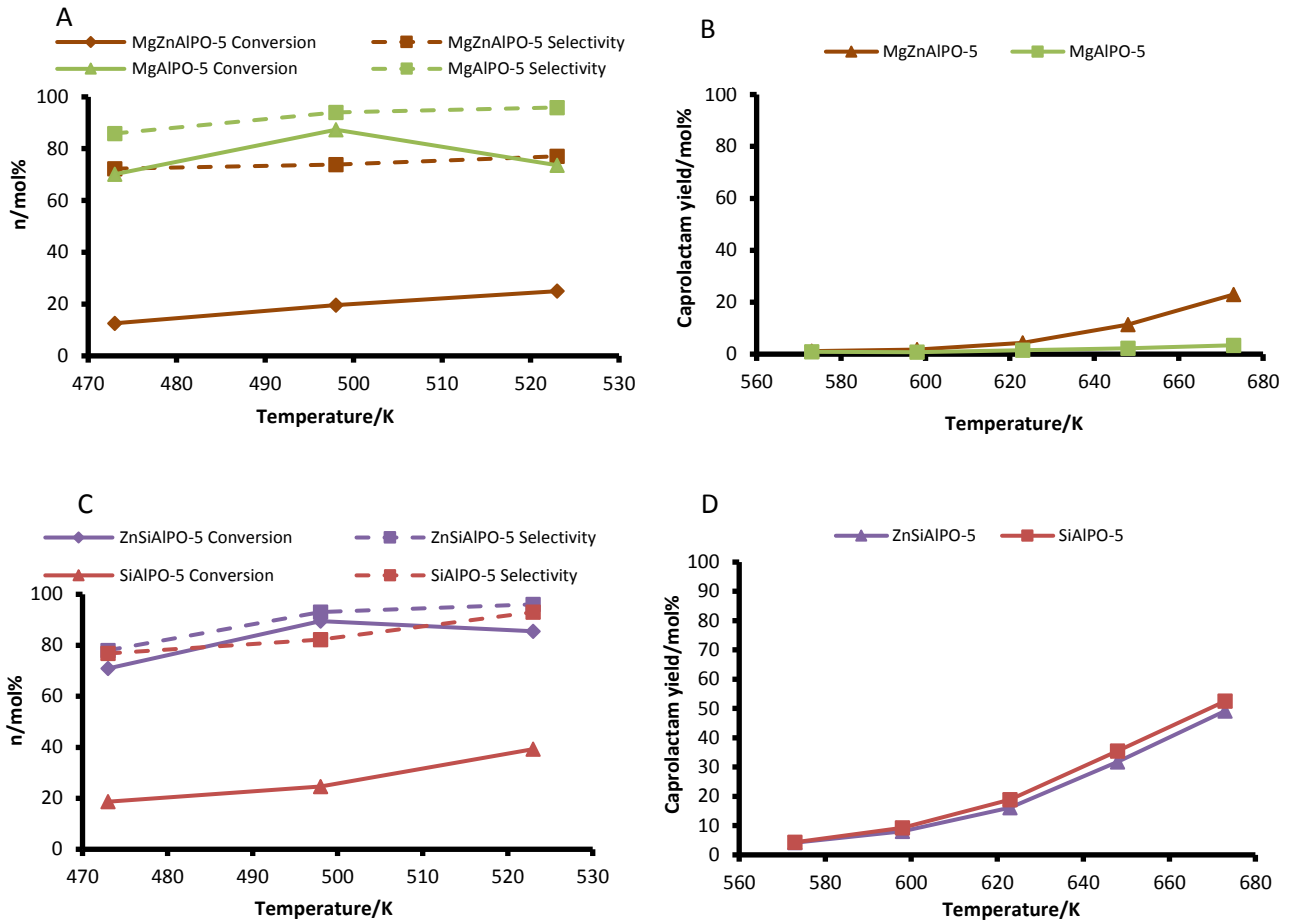

Fig. 5 Activity of Mg, Si and Zn-containing catalysts on the isopropylation of benzene (A & C) and vapour-phase Beckmann Rearrangement (B & D). Conditions: A & C: WHSV of 3.5 hr^{-1}, Helium carrier gas of 10 ml/min, feed 6:1 mole ratio of benzene:isopropanol, temperature as shown. B & D) WHSV 3.3 hr^{-1}, Helium carrier gas flow 20 ml/min, 0.3 g of catalyst, liquid feed 300g/l of cyclohexanone oxime in methanol, temperature as shown.

Thus, despite being inactive, when combined with other metals zinc has been shown to form unique metal-metal interactions. Even though examples existing in the literature of inactive species modulating catalytic behaviour for one specific reaction, such as the addition of Ca^{2+} ions to rare-earth Zeolite-Y for catalytic cracking processes,[31-32] we have shown the ability of inert zinc species to improve two contrasting and distinct acid-catalysed transformations. The reasons for this novel enhancement are currently unclear and will serve as the basis for a more robust characterisation study in future.

Conclusions

The ability to succinctly modify the catalytic activity of an acid active site in nanoporous materials, through the inclusion of a second site, has been established. Further, the requirement for precise pairing of metal sites is emphasised, as different bimetallic combinations are found to succinctly modify the nature of the active site, thereby prompting different catalytic responses to the analogous monometallic systems. We have shown how the dual incorporation of such complementary pairings of dopant-metals can be employed to enhance the activity of monometallic species, for the vapour-phase Beckmann rearrangement of cyclohexanone oxime and in the isopropylation of benzene.

Acknowledgements

We acknowledge Honeywell LLC for funding this project.

Notes and references

1 T. Maschmeyer, F. Rey, G. Sankar and J. M. Thomas, *Nature*, 1995, **378**, 159.
2 A. Thangaraj, R. Kumar and P. Ratnasamy, *J. Catal.*, 1991, **131**, 294.
3 A. T. Bell, *Science*, 2003, **299**, 1688.
4 L. Li, G. D. Li, C. Yan, X. Y. Mu, X. L. Pan, X. X. Zou, K. X. Wang and J. S. Chen, *Angew. Chem. Int. Ed.*, 2011, **36**, 8449.
5 J. Lee, O. K. Farha, J. Roberts, K. A. Scheidt, S. T. Nguyen and J. T. Hupp, *Chem. Soc. Rev.*, 2009, **38**, 1450.
6 J. K. Edwards, B. E. Solsona, P. Landon, A. F. Carley, A. Herzing, C. J. Kiely and G. J. Hutchings, *J. Catal.*, 2005, **236**, 69.

7 S. G. Wettstein, J. Q. Bond, B. M. Alonso, H. N. Pham, A. K. Datye and J. A. Dumesic, *Appl. Catal. B: Environ.*, 2012, **117**, 321.
8 K. Ishii, F. Mizukami, S. Niwa, R. Kutsuzawa, M. Toba and Y. Fujii, *Catal. Lett.*, 1998, **52**, 49.
9 J. Silvestre-Albero, J. C. Serrano-Ruiz, A. Sepulveda-Escribano and F. Rodriguez-Reinoso, *Appl. Catal. A. Gen.*, 2005, **292**, 244.
10 L. Kesavan, R. Tiruvalam, M. H. Ab Rahim, M. I. bin Saiman, D. I. Enache, R. L. Jenkins, N. Dimitratos, J. A. Lopez-Sanchez, S. H. Taylor, D. W. Knight, C. J. Kiely and G. J. Hutchings, *Science*, 2011, **331**, 195.
11 R. D. Adams and B. Captain, *Angew. Chem. Int. Ed.*, 2008, **47**, 252.
12 A. B. Hungaria, R. Raja, R. D. Adams, B. Captain, J. M. Thomas, P. A. Midgley, V. Golovko and B. F. G. Johnson, *Angew. Chem. Int. Ed.*, 2006, **45**, 4782.
13 E. Gianotti, V. N. Shetti, M. Manzoli, J. A. L. Blaine, W. C. Pearl Jr., R. D. Adams, S. Coluccia and R. Raja, *Chem. Eur. J.*, 2010, **16**, 8202.
14 R. Raja, G. Sankar and J.M. Thomas, J. *Am. Chem. Soc.,* 2001, **123**, 8153.
15 R. Raja and J.M. Thomas, *Proc. Natl. Acad. Sci.*, 2005, **39**, 13732.
16 R. Mokaya and M. Poliakoff, *Nature*, 2005, **437**, 1243.
17 P. A. Barrett, G. Sankar, C. R. A. Catlow and J. M. Thomas, *J. Phys. Chem.*, 1996, **100**, 8977.
18 C. S. Blackwell and R. L. Patton, *J. Phys. Chem.*, 1988, **92**, 3965.
19 M. Lefenfeld, R. Raja, A.J. Paterson and M.E. Potter, US Patent 021882, 2010.
20 A. J. Paterson, M.E. Potter, E. Gianotti and R. Raja, *Chem Commun.*, 2011, **47**, 517.
21 M. E. Potter, A. J. Paterson and R. Raja, ACS Catal., 2012, 2, 2446.
22 R. M. Leithall, V. N. Shetti, S. Maurelli, M. Chiesa, E. Gianotti and R. Raja, *J. Am. Chem. Soc.*, 2013, **135**, 2915.
23 Product focus, Chem. Week 7, 2007
24 G. Dahlhoff, J.P.M. Niederer and W.F. Hoelderich, *Catal. Rev. Sci. Eng.*, 2001, **43**, 381.
25 K. S. N. Reddy, B. S. Rao and V. P. Shiralkar, *Appl. Catal. A: Gen.*, 1993, **95**, 53.
26 A. B. Fernandez, M. Boronat, T. Blasco and A. Corma, *Angew. Chem. Int. Ed.*, 2005, **44**, 2370.
27 I. Lezcano-Gonzales, A. Vidal-Moya, M. Boronat, T. Blasco and A. Corma, *Phys. Chem. Chem. Phys.*, 2010, **12**, 6396.
28 S. K. Saha, S. B. Waghmode, H. Maekawa, K. Koruma, Y. Kubota, Y. Sugi, Y. Oumi and T. Sano, *Micro. Meso. Mater.*, 2005, **81**, 289.
29 F. Cora, M. Alfredsson, C.M. Barker, R.G. Bell, M.D. Foster, I. Saadoune, A. Simplerer and C.R.A. Catlow, *J. Solid State Chem.*, 2003, **176**, 496.
30 M.E. Potter, A.J. Paterson, B. Mishra, S.D. Kelly, S.R. Bare, F. Cora, A.B. Levy and R. Raja, *J. Am. Chem. Soc.*, 2015, **137**, 8534.
31 K. J. Chao, L. H. Lin and L. Y. Han, *Stud. Surf. Sci. Catal.*, 1995, **98**, 67.
32 F. Roessner, K. H. Steinberg and H. Winkler, *Zeolites*, 1987, **7**, 47.

Supplementary information

The curious effects of integrating bimetallic active centres within nanoporous architectures for acid-catalysed transformations

Matthew E. Potter[a], Danni Sun[b] and Robert Raja[b*]

[a] *Georgia Institute of Technology, School of Chemical and Biomolecular Engineering, 311 Ferst Drive, Atlanta, GA, 30332-0100, USA.*
[b] *School of Chemistry, University of Southampton, Highfield, Southampton, Hants, SO17 1BJ, UK; E-mail: R.Raja@soton.ac.uk*

Table of contents

Structural characterisation data

Table S1: Full ICP data

System	Al/wt%	P/wt%	Zn/wt%	Mg/wt%	Si/wt%
AlPO-5	18.1	16.7	-	-	-
MgAlPO-5	15.9	20.6	-	0.85	-
ZnAlPO-5	16.4	21.2	2.11	-	-
SiAlPO-5	19.8	14.7	-	-	1.69
MgZnAlPO-5	17.0	22.9	1.86	0.72	-
MgSiAlPO-5	18.0	14.6	-	0.89	1.70
ZnSiAlPO-5	18.7	15.9	1.33	-	1.66

Table S2: XRD parameters, particle size and surface area summary

System	Optimized XRD parameters for P6cc		Particle size/nm	BET SSA/m^2 g^{-1}
	a/Å	c/Å		
AlPO-5	13.69	8.43	56.5	295.1
ZnAlPO-5	13.68	8.34	55.5	165.4
MgAlPO-5	13.71	8.40	55.5	193.3
SiAlPO-5	13.70	8.39	54.8	181.9
MgZnAlPO-5	13.80	8.41	66.3	283.3
MgSiAlPO-5	13.71	8.39	52.6	168.1
ZnSiAlPO-5	13.76	8.40	64.2	236.2

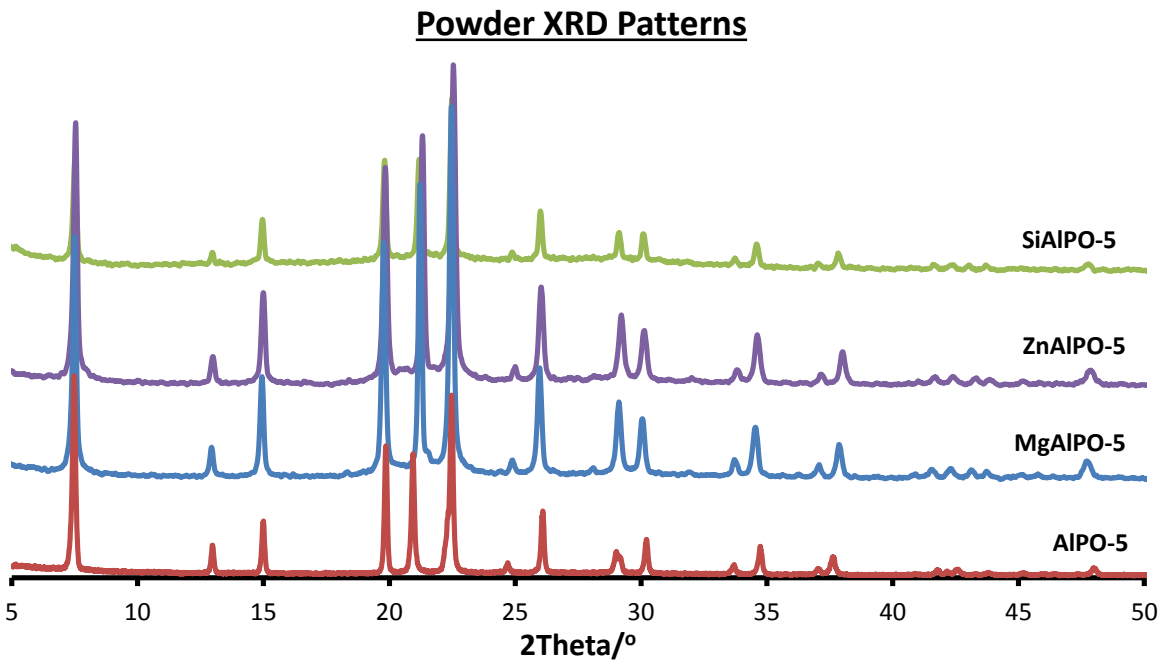

Figure S1: Powder X-ray diffraction pattern of monometallic AlPO-5 systems

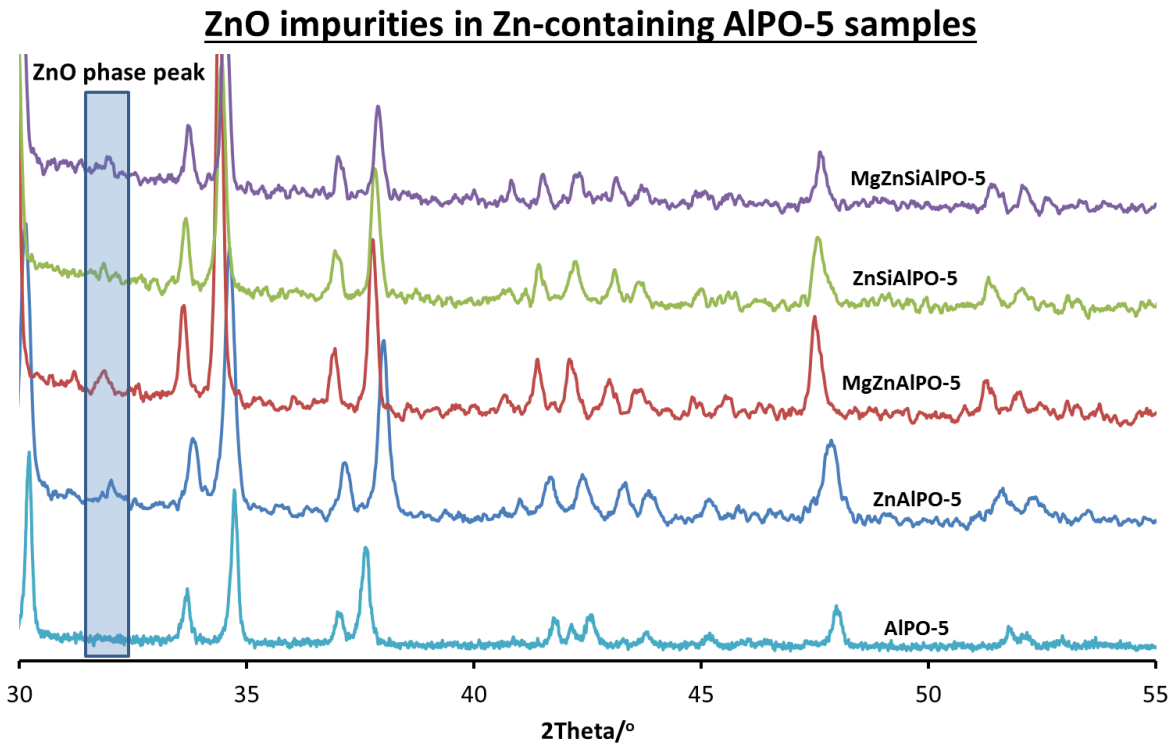

Figure S2: Zoomed XRD pattern of Zn-containing species revealing trace quantities of ZnO hexagonal phase.

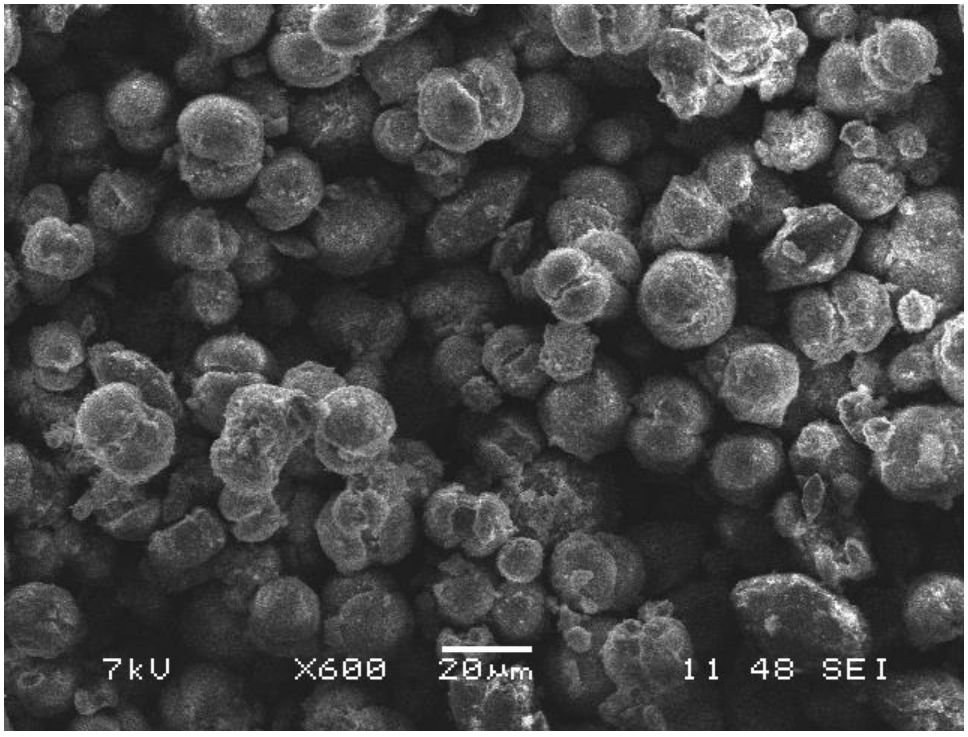

Figure S3: SEM image of monometallic MgAlPO-5

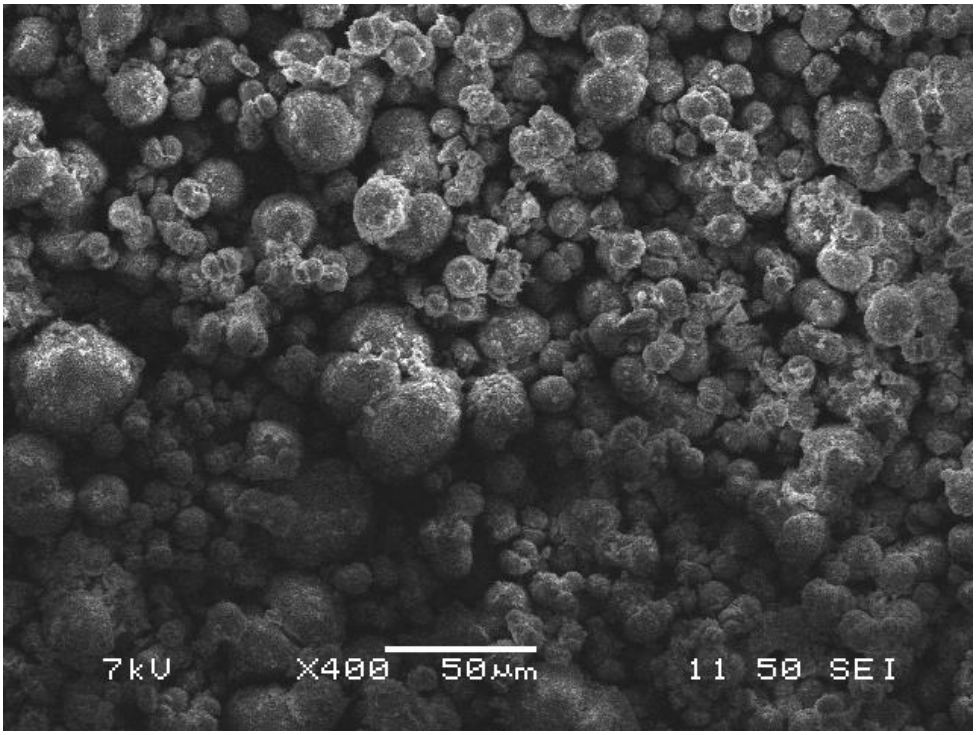

Figure S4: SEM image of monometallic ZnAlPO-5

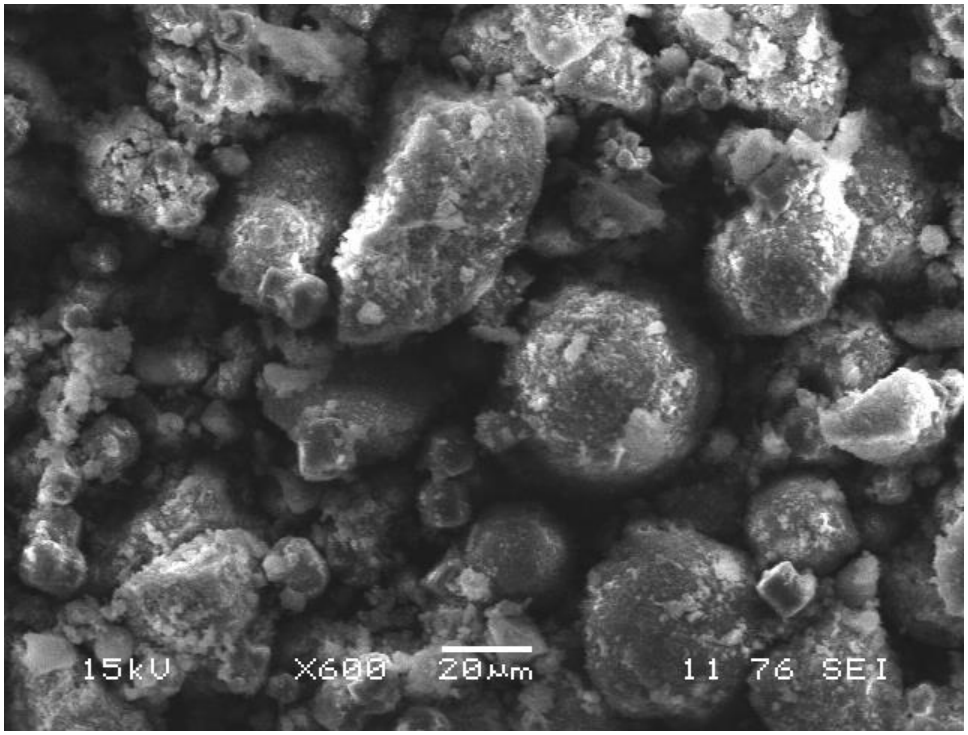

Figure S5: SEM image of monometallic SiAlPO-5

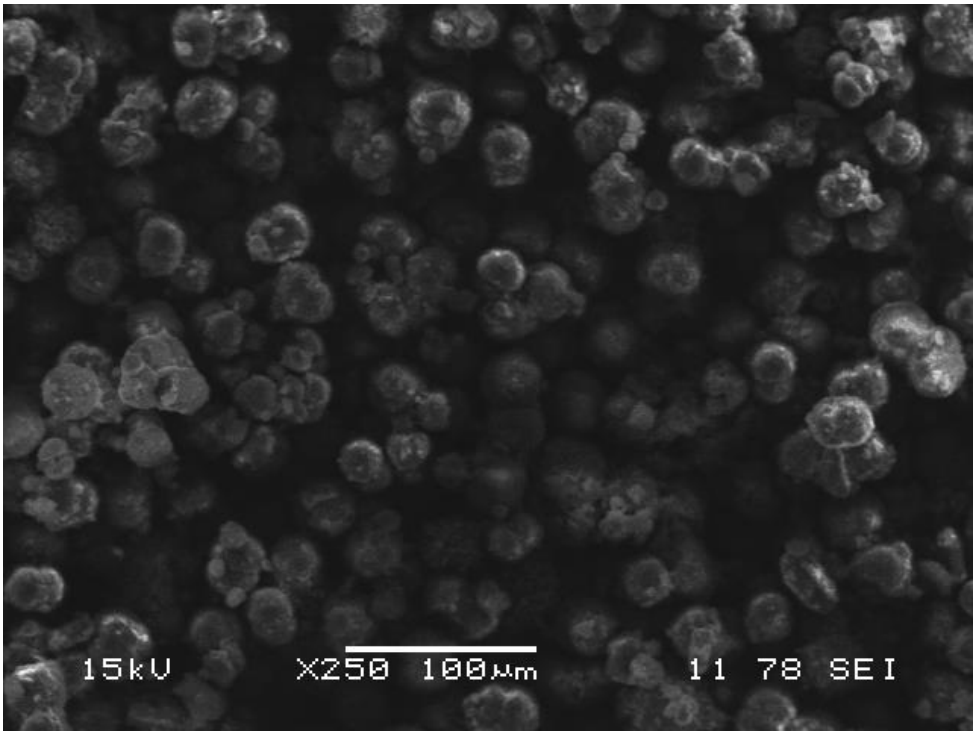

Figure S6: SEM image of bimetallic MgZnAlPO-5

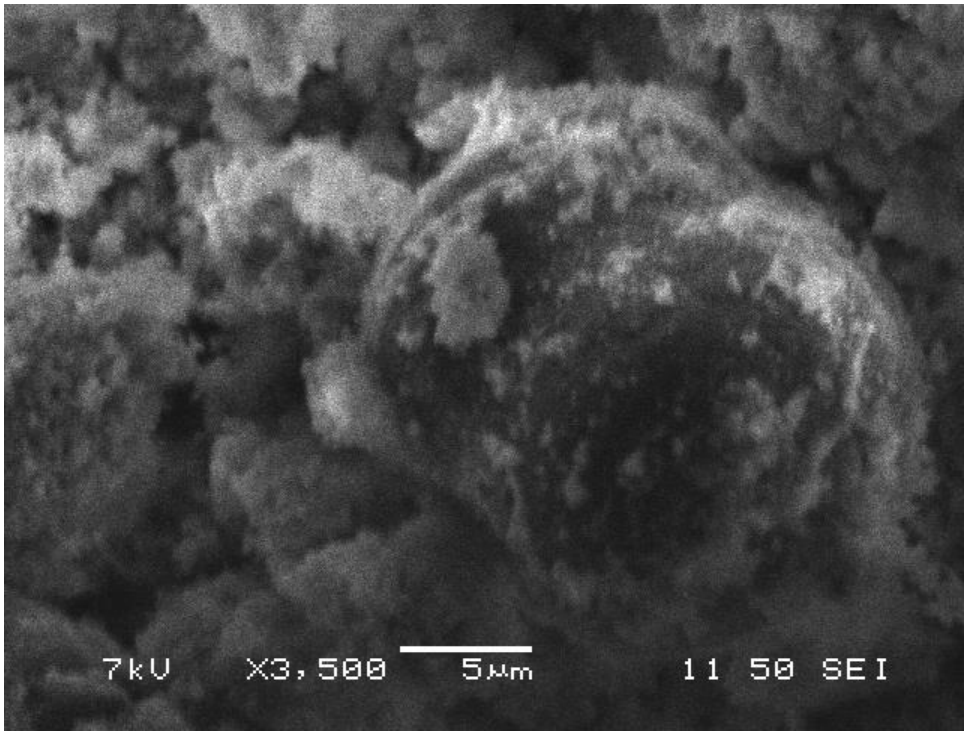

Figure S7: SEM image of bimetallic MgSiAlPO-5

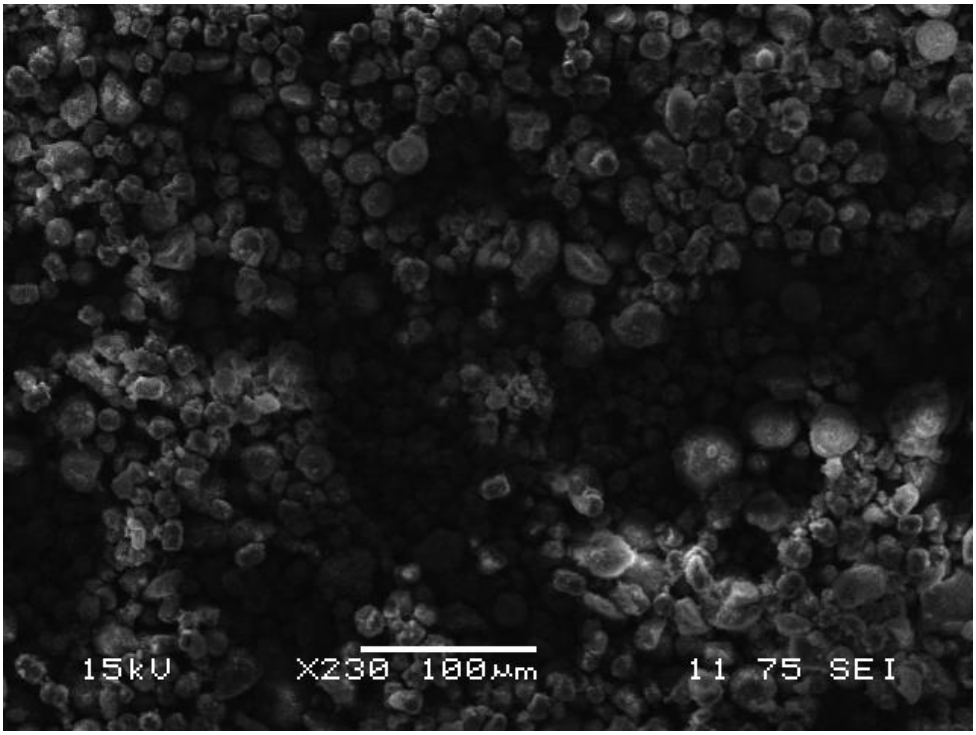

Figure S8: SEM image of bimetallic ZnSiAlPO-5

Full catalysis data

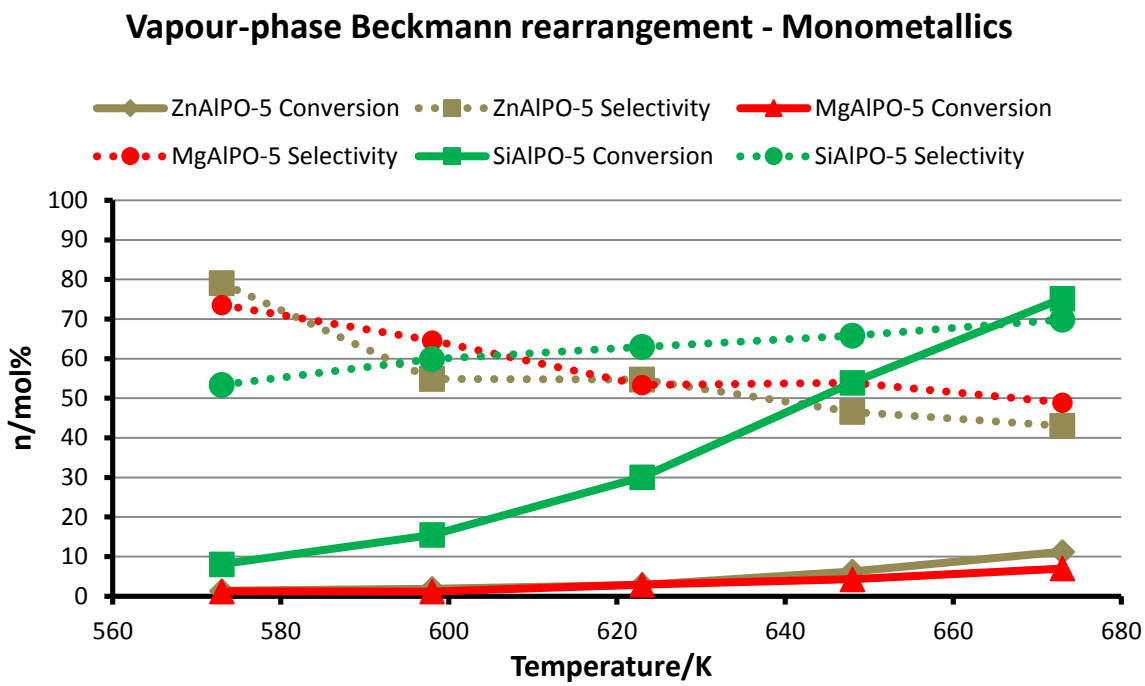

Figure S9: Full catalytic data for the vapour-phase Beckmann rearrangement of cyclohexanone oxime using monometallic AlPO-5 systems. Reaction conditions: WHSV 3.3 hr^{-1}, Helium carrier gas flow 20 ml/min, 0.3 g of catalyst, liquid feed 300g/l of cyclohexanone oxime in methanol, temperature as shown.

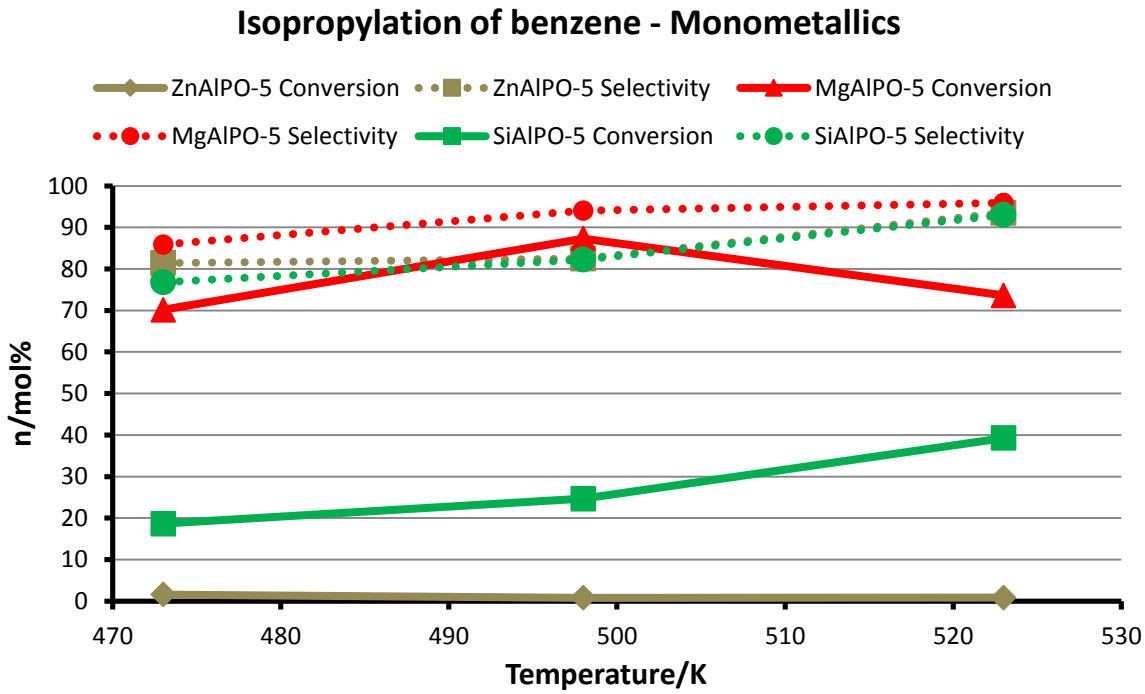

Figure S10: Full catalytic data for the isopropylation of benzene using monometallic AlPO-5 systems. Reaction conditions: WHSV of 3.5 hr^{-1}, Helium carrier gas of 10 ml/min, feed 6:1 mole ratio of benzene:isopropanol, temperature as shown.

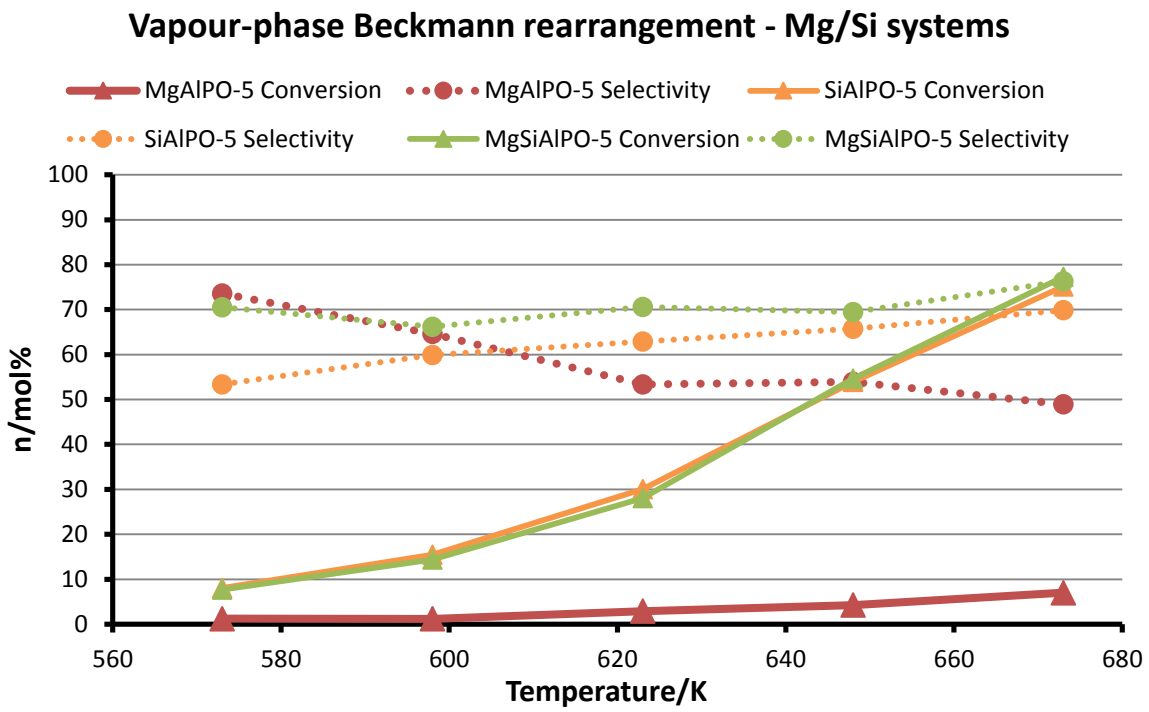

Figure S11: Full catalytic data for the vapour-phase Beckmann rearrangement of cyclohexanone oxime using Mg and Si-containing AlPO-5 systems. Reaction conditions: WHSV 3.3 hr^{-1}, Helium carrier gas flow 20 ml/min, 0.3 g of catalyst, liquid feed 300g/l of cyclohexanone oxime in methanol, temperature as shown

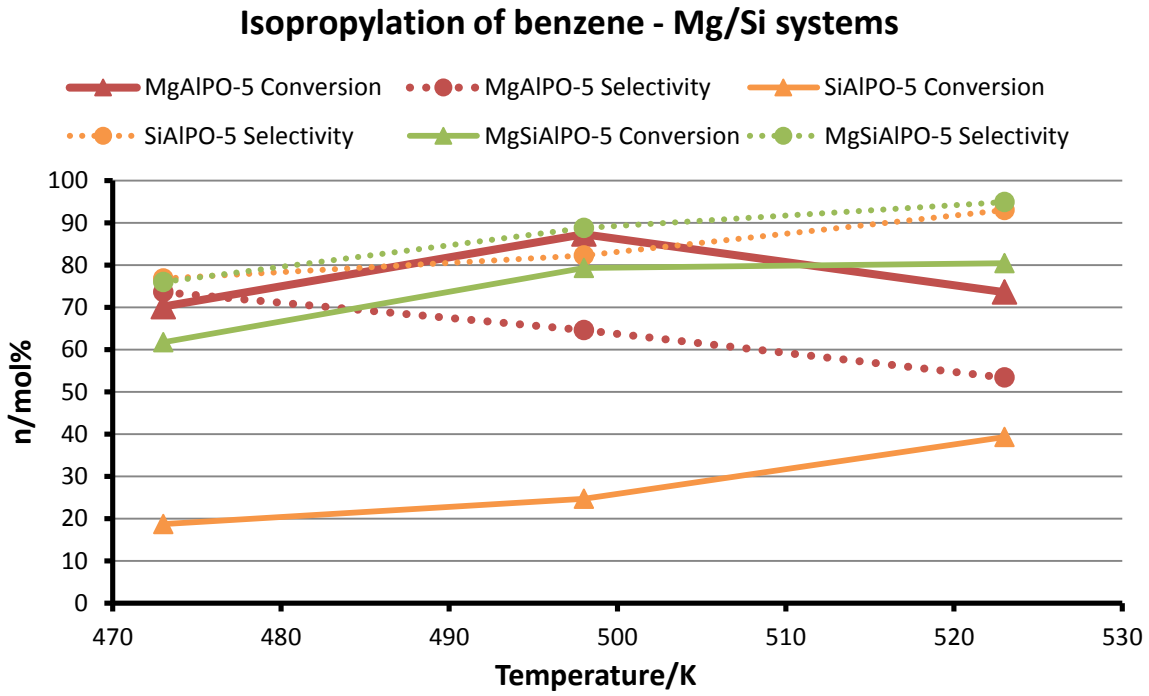

Figure S12: Full catalytic data for the isopropylation of benzene using Mg and Si-containing AlPO-5 systems. Reaction conditions: WHSV of 3.5 hr^{-1}, Helium carrier gas of 10 ml/min, feed 6:1 mole ratio of benzene:isopropanol, temperature as shown.

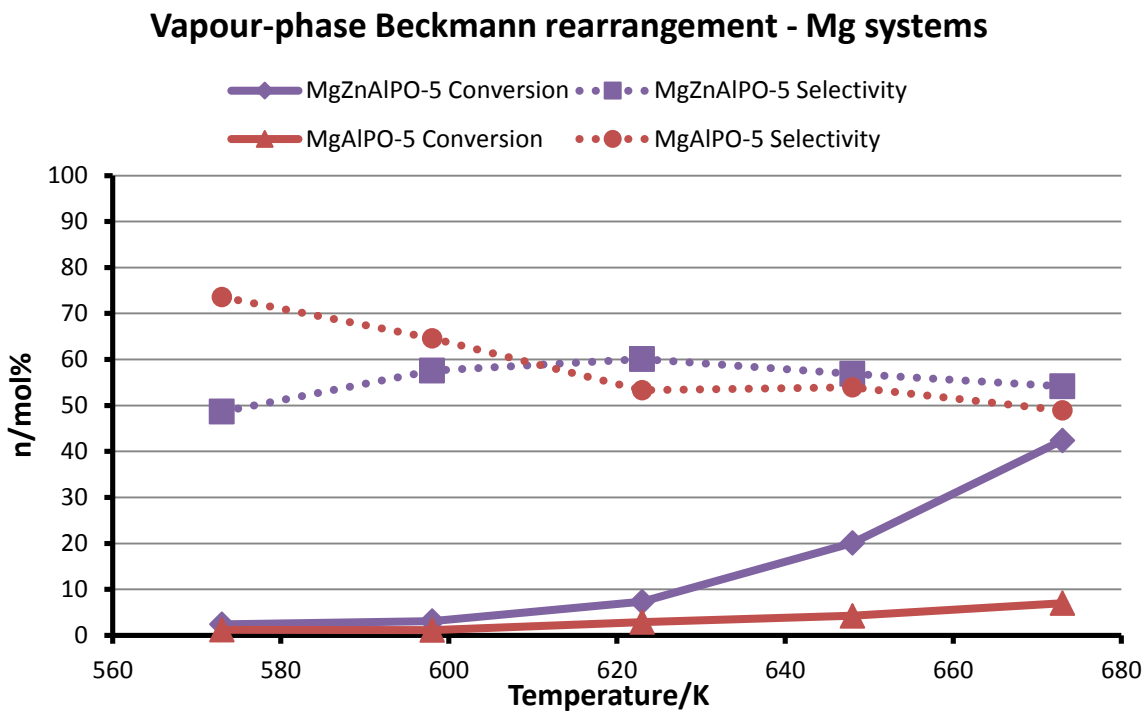

Figure S13: Full catalytic data for the vapour-phase Beckmann rearrangement of cyclohexanone oxime using Mg-containing AlPO-5 systems. Reaction conditions: WHSV 3.3 hr^{-1}, Helium carrier gas flow 20 ml/min, 0.3 g of catalyst, liquid feed 300g/l of cyclohexanone oxime in methanol, temperature as shown.

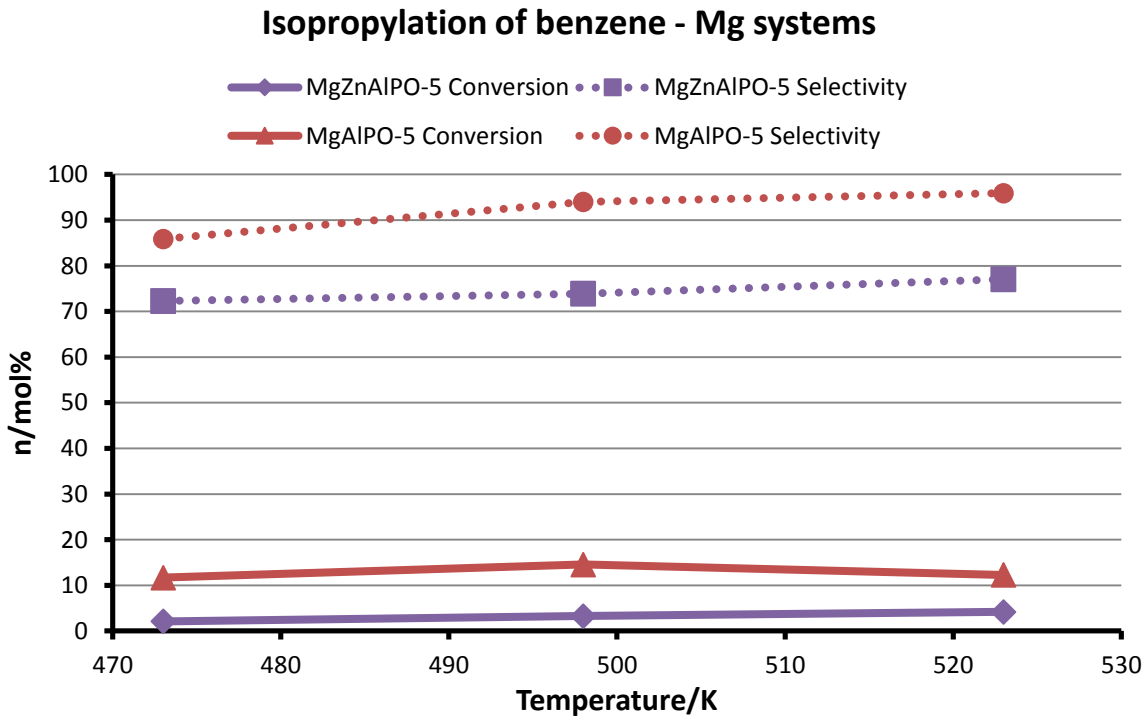

Figure S14: Full catalytic data for the isopropylation of benzene using Mg-containing AlPO-5 systems. Reaction conditions: WHSV of 3.5 hr^{-1}, Helium carrier gas of 10 ml/min, feed 6:1 mole ratio of benzene:isopropanol, temperature as shown.

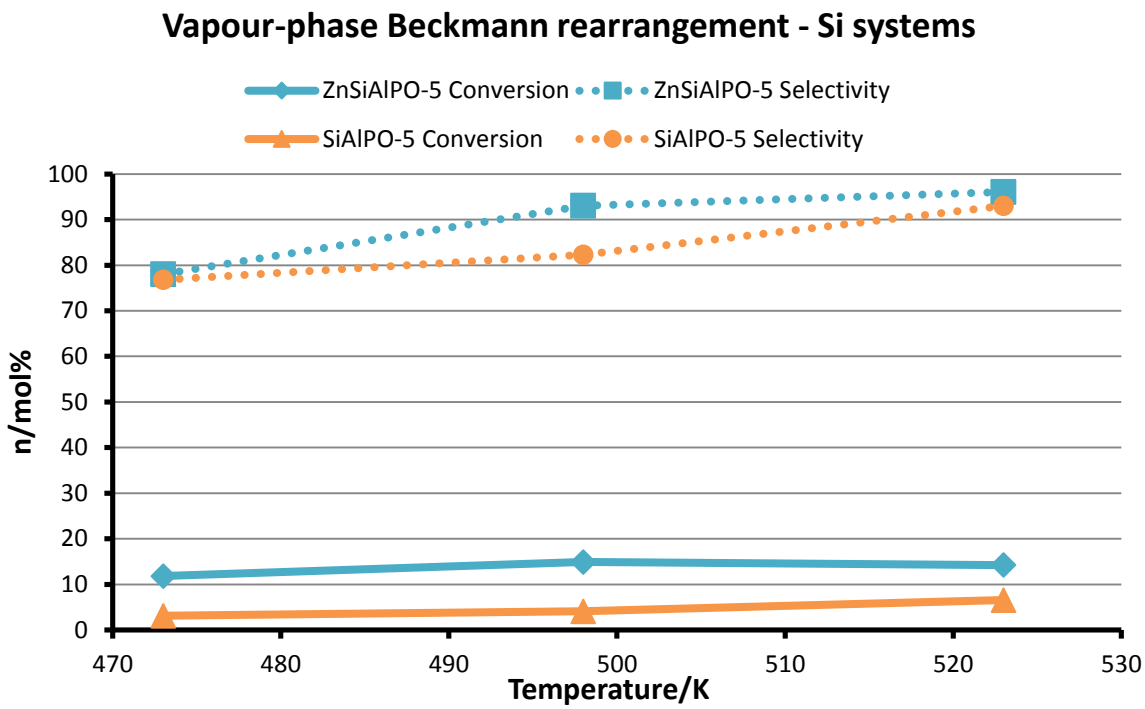

Figure S15: Full catalytic data for the vapour-phase Beckmann rearrangement of cyclohexanone oxime using Si-containing AlPO-5 systems. Reaction conditions: WHSV 3.3 hr^{-1}, Helium carrier gas flow 20 ml/min, 0.3 g of catalyst, liquid feed 300g/l of cyclohexanone oxime in methanol, temperature as shown.

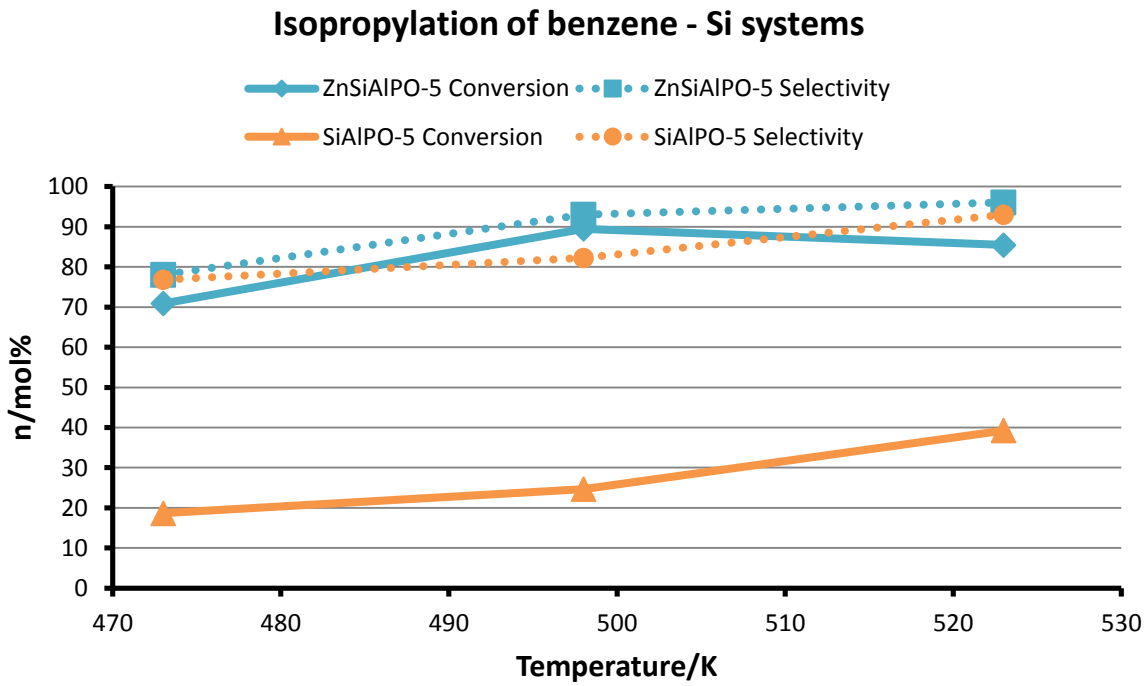

Figure S16: Full catalytic data for the isopropylation of benzene using Si-containing AlPO-5 systems. Reaction conditions: WHSV of 3.5 hr^{-1}, Helium carrier gas of 10 ml/min, feed 6:1 mole ratio of benzene:isopropanol, temperature as shown.

Mechanistic pathways

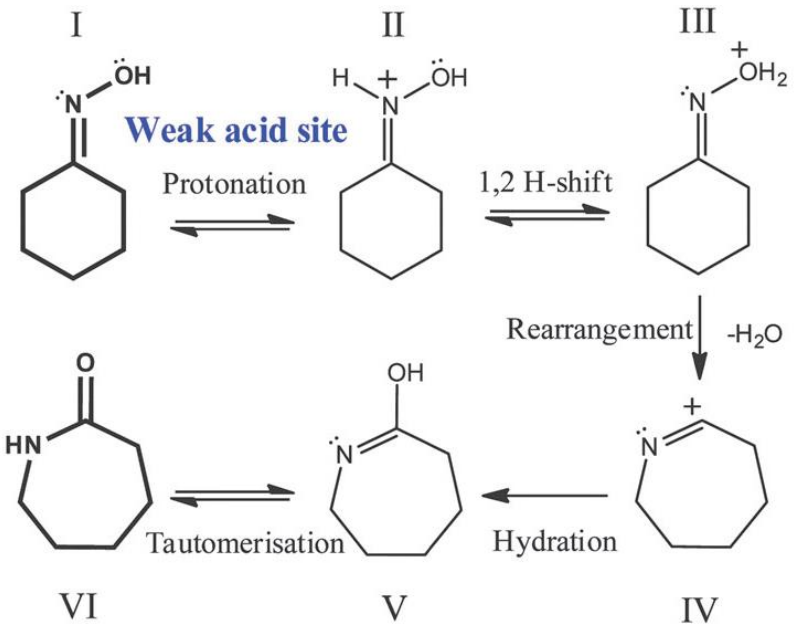

Figure S17: Mechanistic pathway of the Beckmann rearrangement of cyclohexanone oxime.

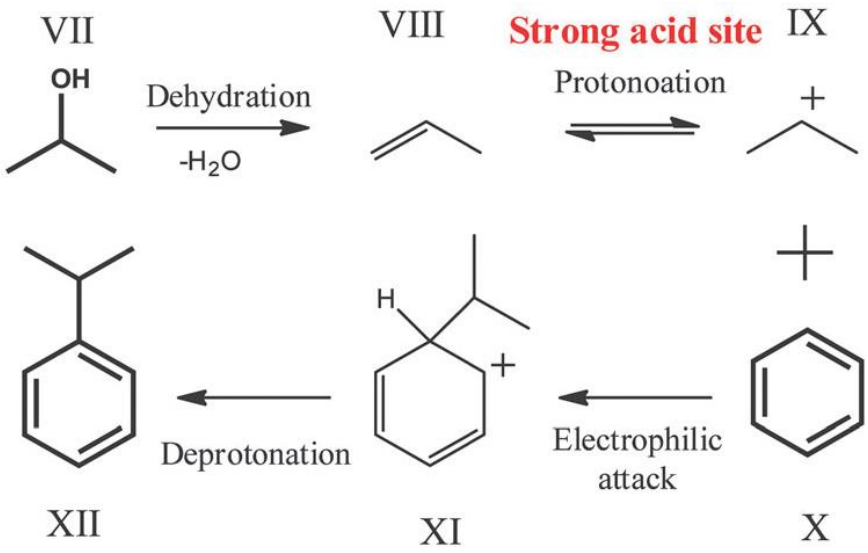

Figure S18: Mechanistic pathway of the isopropylation of benzene to cumene.